remote sensing

MDPI

Article

Individual Tree Segmentation Based on Seed Points Detected by an Adaptive Crown Shaped Algorithm Using UAV-LiDAR Data

Jiao Yu [1,2,3,†], Lei Lei [1,2,3,†] and Zhenhong Li [1,2,4,*]

[1] College of Geological Engineering and Geomatics, Chang'an University, Xi'an 710054, China; 2021126058@chd.edu.cn (J.Y.); 2020026022@chd.edu.cn (L.L.)
[2] Key Laboratory of Loess, Xi'an 710054, China
[3] Big Data Center for Geosciences and Satellites, Xi'an 710054, China
[4] Key Laboratory of Ecological Geology and Disaster Prevention, Ministry of Natural Resources, Xi'an 710054, China
* Correspondence: zhenhong.li@chd.edu.cn
† These authors contributed equally to the work.

Abstract: Unmanned aerial vehicle–light detection and ranging (UAV-LiDAR) provides a convenient and economical means of forest data acquisition that can penetrate canopy gaps to obtain abundant ground information, offering huge potential in forest inventory. Individual tree segmentation is a prerequisite to obtain individual tree details but is highly dependent on the accuracy of seed point detection. However, most of the existing methods, such as the local maximum (LM) and CHM-based methods, are strongly dependent on the window size, and, for individual tree segmentation, they can result in over-segmentation and under-segmentation, especially in natural forests. In this paper, we propose an adaptive crown shaped algorithm for individual tree segmentation without consideration of the window size. It was implemented in four plots with different forest types and topographies (i.e., planted coniferous forest with flat terrain, coniferous forest with sloping terrain, mixed forest with flat terrain and broadleaf forest with flat terrain). First, the normalized point clouds were rotated and blocked at multiple angles to extract the surface points of the forest. Then, the crown boundaries were delineated by analyzing the crown profiles to extract the treetops as seed points. Finally, a region growing method based on seed points was applied for individual tree segmentation. Our results showed that the recall, precision and F1-score of seed point detection reached 91.6%, 95.9% and 0.94, respectively, and that the accuracy rates for individual tree segmentation for the four plots were 87.7%, 80.6%, 73.2% and 70.5%, respectively. Our proposed method can effectively detect seed points via the adaptive crown shaped algorithm and reduce the impacts of elongated branches by applying distance thresholds between trees, enhancing the accuracy of seed point detection and subsequently improving the precision of individual tree segmentation. In addition, the proposed algorithm demonstrated superior performance in comparison to LM and CHM-based methods for the calculation of seed points, as well as outperforming PCS in individual tree segmentation. The proposed method demonstrates effectiveness and feasibility in dense forests and natural forests, providing an important reference for future research on seed point detection and individual tree segmentation.

Keywords: UAV-LiDAR; individual tree segmentation; seed point detection; different forest types and topographies

Citation: Yu, J.; Lei, L.; Li, Z. Individual Tree Segmentation Based on Seed Points Detected by an Adaptive Crown Shaped Algorithm Using UAV-LiDAR Data. *Remote Sens.* **2024**, *16*, 825. https://doi.org/10.3390/rs16050825

Academic Editor: Lars T. Waser

Received: 28 December 2023
Revised: 9 February 2024
Accepted: 17 February 2024
Published: 27 February 2024

1. Introduction

Forests are essential in preserving the biodiversity and ecological balance in terrestrial ecosystems, serving as a source of fundamental materials for human life and production [1–3]. Conducting forest resource surveys is crucial for sustainable development. It not only establishes a foundational dataset for forestry scientific research but also provides crucial evidence for the management and conservation of ecological environments [4–6]. Traditional forest inventories rely on field surveys, typically facilitated by measuring tools to

acquire forest structural features, including altimeters for tree height, total stations for position [7], calipers for DBH and so on. Although this method can obtain detailed and accurate information on individual trees, it is time-consuming, labor-intensive and difficult to apply in large areas [8,9]. Traditional remote sensing technologies acquire optical images of forests (hyperspectral, multispectral and radar images, etc.) by satellite or aerial photography, and these images are interpreted to extract information about individual trees [10]. This method can effectively provide forest information over large areas, but two-dimensional (2D) images lack information from below the canopy and hence fail to fully exhibit the three-dimensional (3D) structural features of forests [11,12]. Close-range photogrammetry based on structure from motion algorithms (SFM) can be used to produce a 3D forest model using photographic information and generate a large number of point clouds [13]. While this method can provide 3D information about individual trees, its accuracy depends on the quality of the photographs, with the computational efficiency decreasing as the volume of data increases [14].

With the emergence of remote sensing and unmanned aerial vehicle (UAV) technologies, UAV-LiDAR is becoming increasingly popular in forest surveys due to its low cost and easy operation [15,16]. UAV-LiDAR, as an active remote sensing technique, generates point clouds with 3D information about the forest by emitting laser pulses into the leaves and branches [17]. This method not only provides high-precision 3D information on large-area forests but also has the capability to penetrate vegetation gaps to obtain understory information [18–20].

Individual tree segmentation is a key step in obtaining the structural features of trees. Existing individual tree segmentation algorithms can be categorized into raster-based methods, point cloud-based methods and hybrid methods. Raster-based methods segment individual trees using image processing approaches on a digital surface model (DSM) or canopy height model (CHM). Common methods include the watershed algorithm [21], marker-controlled watershed algorithm [22], region growing [23], template matching [24] and valley following [25]. The CHM is derived by subtracting the digital elevation model (DEM) from the DSM [26]. Chen et al. (2006) proposed a variable window local maximum method to detect treetops and the marker-controlled watershed algorithm was employed to achieve canopy segmentation in sparse grassland forests [27]. Koch et al. (2006) integrated a pouring approach with knowledge based on tree shapes to detect the crown edges for individual crown segmentation [5]. Wu et al. (2016) developed a graph-theory-based localized contour tree method, combining geometric and topological features to extract the hierarchical structures of tree crowns for individual tree segmentation [28]. Compared to complex point clouds, raster data have a simple structure. Therefore, individual tree segmentation methods based on raster data have high computational efficiency and accuracy in simple forest environments [29]. However, the accuracy of individual tree segmentation depends significantly on the spatial resolution of the raster data [30]. Additionally, the transformation of point clouds into a raster can lead to the loss of 3D structural information and some forest details, posing challenges in detecting understory vegetation and the boundaries of intertwining trees in complex forests [31].

Point-cloud-based methods cluster the LiDAR points of individual trees based on the normalized point cloud using the spatial structure features of the point cloud [32]. There are several popular methods, such as region growing [12,33], mean shift [3], K-means [34], normalized cut [35] and the density-based spatial clustering of applications with noise (DBSCAN) [36]. Li et al. (2012) proposed a top-down region growing algorithm, which took into account the crown shape and the distance relationship between trees to achieve individual tree segmentation [33]. Yan et al. (2020) presented a self-adaptive mean shift tree segmentation method that can automatically estimate the optimal kernel bandwidth without prior knowledge of the tree crown size [37]. Hao et al. (2022) developed a hierarchical region-merging algorithm that initially performed over-segmentation based on the local density, followed by a stepwise optimal merging process to achieve the final segmentation [4]. Point-cloud-based methods can detect secondary layers in complex

forests using the 3D structural information of forests. Compared with raster-based methods, this reduces under-segmentation and can obtain finer individual tree parameters [38]. However, the method is time-consuming due to the large number of point clouds, making it more demanding in terms of computer performance.

Hybrid methods combine point-cloud-based methods or raster-based methods with the spatial characteristics of the point cloud to improve the accuracy of individual tree segmentation. Paris et al. (2016) proposed an algorithm that combined CHM analysis with point cloud space analysis [39]. This approach successfully detects crowns missed by the CHM method by analyzing the horizontal profile of the forest, thereby improving the detection rate of secondary layers. Yang et al. (2020) presented an individual tree segmentation algorithm based on the watershed algorithm and 3D spatial distribution analysis [40]. The trees were initially segmented by the marker-controlled watershed algorithm, followed by a multidirectional 3D contour analysis of the single tree to detect the positions of potential treetops. Finally, fine segmentation of the forest has been achieved using K-means. Ma et al. (2020) proposed an individual tree segmentation algorithm based on a region growing algorithm and crown morphological structures [41]. The initial segmentation was performed using the region growing algorithm, and under-segmentation was detected by contour analysis. This combined approach significantly enhanced the detection rate of individual trees compared to using the region growing algorithm alone. Compared to point-cloud-based methods and raster-based methods, these methods improve the detection rate of individual trees—especially the secondary layers that are obscured by the upper canopy. However, they retain the limitations of the single method.

Although numerous methods have been proposed in recent years to improve the accuracy of individual tree segmentation, the process remains challenging. The inaccurate seed points and unclear crown boundaries can often lead to over-segmentation and under-segmentation, especially in natural forests. The accuracy of seed point detection can have an influence on individual tree segmentation. The traditional methods (e.g., local maximum method) are strongly dependent on the window size [42,43]. If the window is too large, the treetops of small trees may be overlooked, and if it is too small, the tops of elongated branches are likely to be misidentified as seed points. In this study, we propose an individual tree segmentation method based on seed point detection using an adaptive crown shaped algorithm. Our method is not dependent on the window size. It performs a profile analysis of a circle centered on the local maximum to delineate and mark initial crowns, which can effectively reduce the impact of higher points on seed point detection.

2. Materials

2.1. Study Area

The study area was located at the Taibai Mountain Experimental Base in Mei County, Baoji City, Shaanxi Province. Four plots with different forest types and topographies were used in this study. Detailed information on the four experimental plots (including the forest type, slope, area, stem density and difference) is presented in Table 1. Plots 1, 3 and 4 were situated on flat terrain with gentle slopes of approximately 1°, 6° and 5°, respectively. Unlike the others, plot 2 was located on one side of a hill, with a steeper slope of 36°, and the trees grew in the direction of increasing elevation. The terrain plays a significant role in shaping the growth and distribution of trees. Owing to the effects of slope and elevation, the forest on sloped terrain exhibits a lower tree density compared to flat areas. Figure 1 depicts the location of the study area with optical images of the experimental plots.

Table 1. Detailed information on the four experimental plots.

Plot	Forest Type	Slope	Area (m^2)	Stem Density (Plants/ha)	Difference
P1	Planted coniferous forest	1°	277.98	5540	Trees grow evenly.
P2	Coniferous forest	36°	3021.74	460	Trees grow randomly, with little variation in height.
P3	Mixed forest	6°	4884.62	260	Conifers grow better, with large height differences between trees.
P4	Broadleaf forest	5°	2107.84	612	Trees grow evenly and randomly.

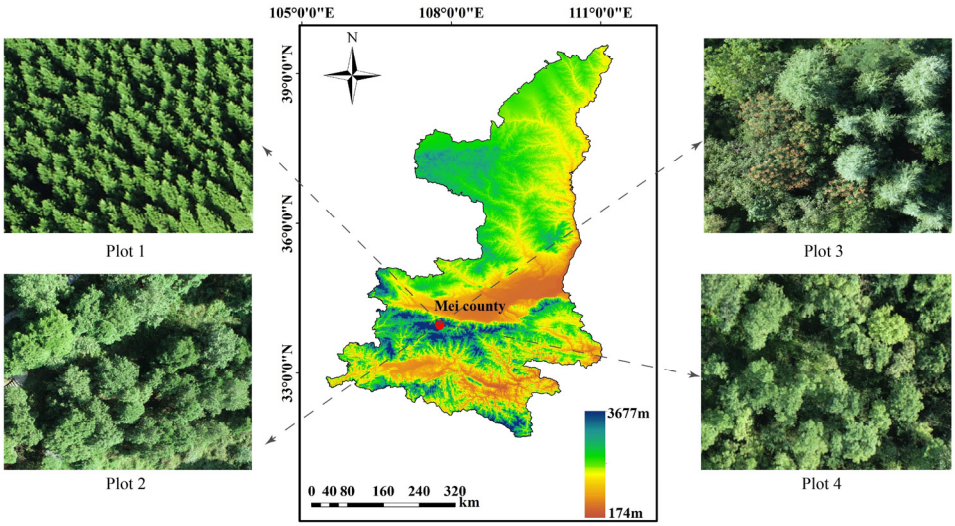

Figure 1. Location of the study area with optical images of the four experimental plots.

2.2. Data Collection

2.2.1. UAV-LiDAR Data

The UAV-LiDAR data were collected on 30 September 2021, using the Zenmuse L1 system (DJI Co., Shenzhen, Beijing), flown at 100 m above ground level, with a flight speed of 5 $m \cdot s^{-1}$. The Zenmuse L1 system has a vertical scanning accuracy of 5 cm and a horizontal scanning accuracy of 10 cm, respectively [44]. In the experimental area, a lateral overlap rate of 50% was employed, and a total of four scans were conducted over the study area to improve the point cloud density. These scans included one orthographic scan and three oblique scans at a tilt angle of -60° in various directions (Table 2). Each scan utilized a multi-route approach to collect data, with an "S-shaped" flight pattern. Figure 2 depicts the details of the UAV-LiDAR data collection. During the collection process, the scanning frequency was 160 kHz, with a measurement speed of 240,000 points/s.

Table 2. Detailed information of four scans.

	Scanning Mode	Direction	Speed (m/s)	Height (m)	Point Density (pts/m^2)
1	orthographic scan	North–South	5	100	197
2	oblique scan at −60°	South–North	5	100	197
3	oblique scan at −60°	West–East	5	100	197
4	oblique scan at −60°	East–West	5	100	197

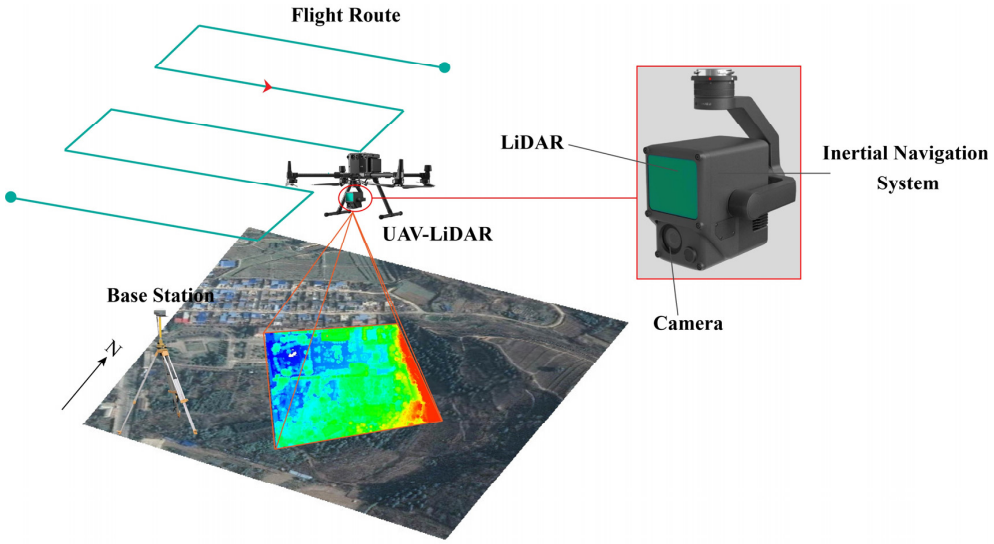

Figure 2. Schematic diagram of UAV-LiDAR data collection.

2.2.2. Measured Data

In this experiment, RGB data were collected, which have rich texture features. When combined with point cloud data for visual interpretation, they allow for the clearer determination of treetop positions and crown boundaries to validate the precision of seed point detection and individual tree segmentation (Figure 3). Furthermore, the tree height (H), crown diameter (CD) and crown projection area (CPA) were measured on the point clouds of individual trees to evaluate the accuracy of the geometric feature extraction. Table 3 shows the measured parameters of the four plots.

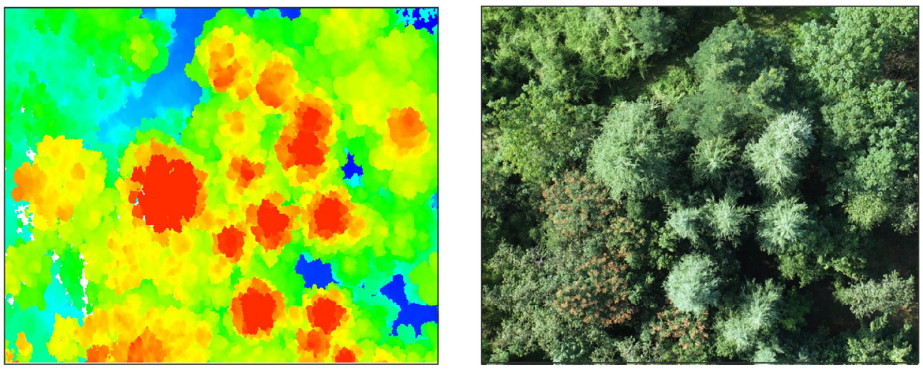

(a) (b)

Figure 3. Point cloud and RGB optical image of mixed forest acquired by UAV-LiDAR: (**a**) point cloud of forest; (**b**) RGB optical image.

Table 3. Parameters of four plots.

Plot	Number	Mean H (m)	Min H (m)	Max H (m)	Max CD (m)	Mean CD (m)	Mean CPA (m^2)
P1	154	9.094	5.750	11.189	3.232	1.770	1.717
P2	139	11.591	5.647	14.900	6.980	4.635	13.973
P3	127	12.299	5.689	20.312	14.631	7.101	29.844
P4	129	8.115	5.688	11.525	9.668	4.727	14.195

2.3. Data Preprocessing

The collected raw data, including trajectory calculation and stitching, were processed using the DJI Terra V3.1.2 software (http://www.dji.com/ (accessed on 2 October 2021)) to generate point clouds, achieving stitching accuracy of approximately 0.21 m. The point clouds were denoised using the Statistical Outlier Removal (SOR) algorithm in the CloudCompare V2.13 software (http://www.cloudcompare.org/ (accessed on 4 November 2021)), employing a parameter setting of 50 for neighbor points and 1.0 m for standard deviation.

In order to reduce the influence of the terrain relief, the point cloud was normalized. The improved progressive TIN densification (IPTD) algorithm [45] was used to separate the ground and non-ground points, and inverse distance weighted (IDW) interpolation was performed on the ground points to generate a DEM with a pixel size of 0.5 m. The non-ground points were then normalized by subtracting the corresponding DEM value from the elevation of the non-ground points. Finally, the point clouds of the four plots were cropped.

3. Methods

3.1. An Adaptive Crown Shaped Algorithm for Individual Tree Segmentation

Treetops—defined as seed points—are the key foundation of individual tree segmentation. Tree crowns may overlap in dense forests; however, there are gaps between treetops, making them usable as feature points in individual tree segmentation [33]. To improve the accuracy of individual tree segmentation, this study proposes an individual tree segmentation method based on the seed points detected by an adaptive crown shaped algorithm, including the following steps: (1) rotating and blocking the normalized point clouds at multiple angles to extract the surface points of the forest; (2) identifying crown boundaries by analyzing the profiles of the surface points and delineating the crowns to extract treetops as seed points; (3) removing the false seed points; and (4) segmenting individual trees using the region growing algorithm based on seed points. A flow chart is shown in Figure 4.

3.1.1. Extraction of Crown Surface Points

The forest point clouds in the study area consist of millions of points with coordinate information. Therefore, extracting seed points directly from these point clouds would impose a substantial computational burden. The surface points of the crown not only preserve its shape characteristics but also facilitate data simplification. Therefore, the crown surface points were extracted for seed point detection in order to enhance the computational efficiency.

The point clouds were initially divided into uniformly spaced blocks along the X-axis (Figure 5(a1)). Subsequently, each block was projected onto the YOZ plane (Figure 5(b1)). Then, the highest point within each interval of the Y-axis was selected as the profile point of the block in the YOZ plane. Finally, all the profile points from the blocks were merged to generate the surface points of the crown (Figure 5(c1)).

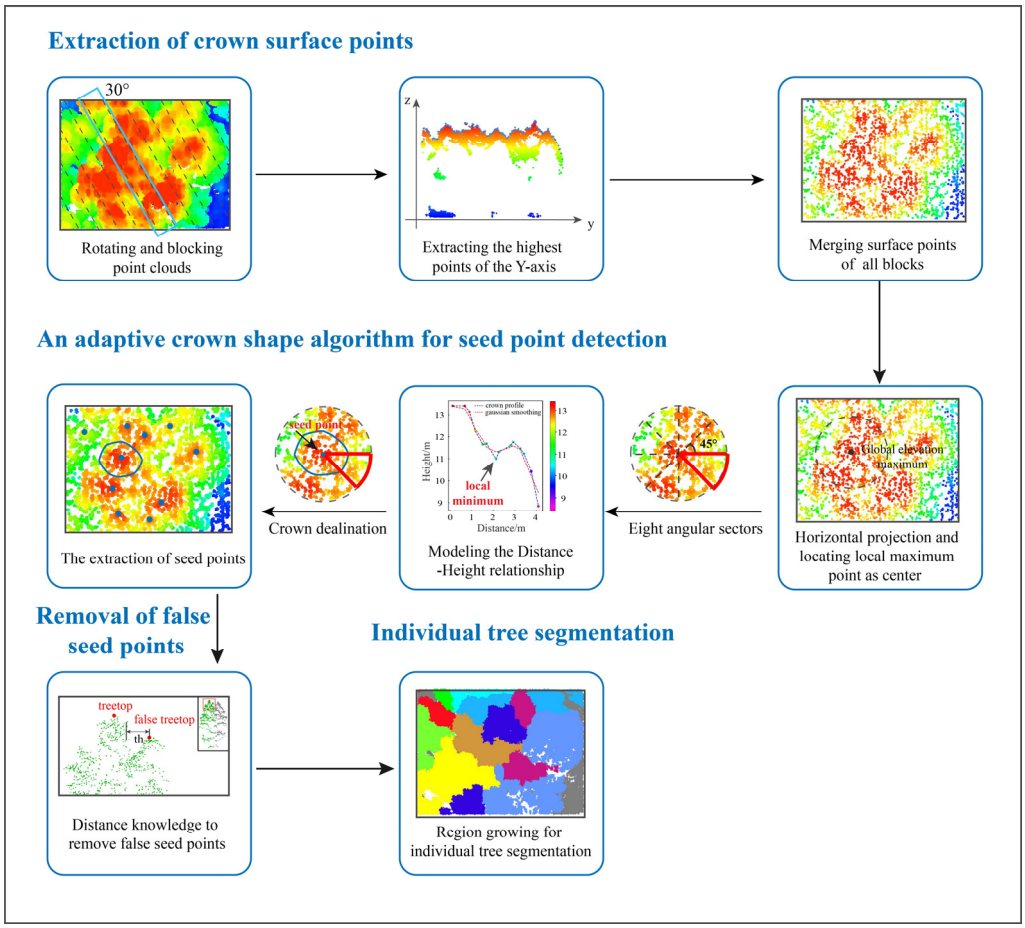

Figure 4. Flow chart of proposed method.

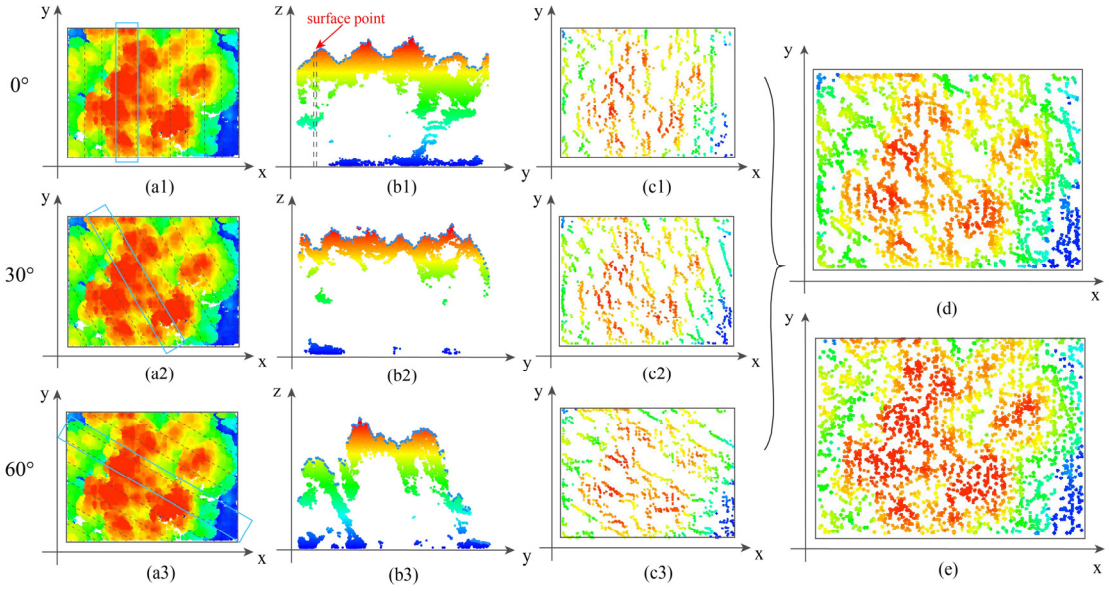

Figure 5. Extraction of crown surface points and merged results from multiple angles. Different colors represent different elevations. (**a1**–**c1**), (**a2**–**c2**) and (**a3**–**c3**) show the process of extracting crown surface points at 0°, 30° and 60°, respectively. (**d**) Merged results of surface points at 0°, 30° and 60°. (**e**) Merged results of surface points of all angles.

However, the surface points extracted from a single angle lack some canopy information. To obtain more complete crown surface points, the point clouds were rotated at 30°

intervals centered on the origin, which was the bottom left corner of the plot. Then, surface points were extracted at 0°, 30°, 60°, 90°, 120° and 150°, respectively. After merging these points from different angles, duplicate points were subsequently eliminated to generate a forest surface without losing the detailed crown features (Figure 5e). The extracted crown surface points at 0°, 30° and 60°, and the merged results, are shown in Figure 5.

3.1.2. Adaptive Crown Shaped Algorithm for Seed Point Detection

The projection of the crown on the plane resembles an ellipse due to its irregular shape, so a circle with a fixed radius cannot represent the actual canopy. If the radius is too large, adjacent treetops may be included within the target tree, resulting in the missed detection of seed points; if the radius is too small, points that are not included in the target tree may be misidentified as treetops, potentially resulting in the detection of false seed points. Therefore, an adaptive crown shaped algorithm for seed point detection based on crown surface points was employed to accurately extract seed points. Figure 6 shows the workflow for the extraction of seed points.

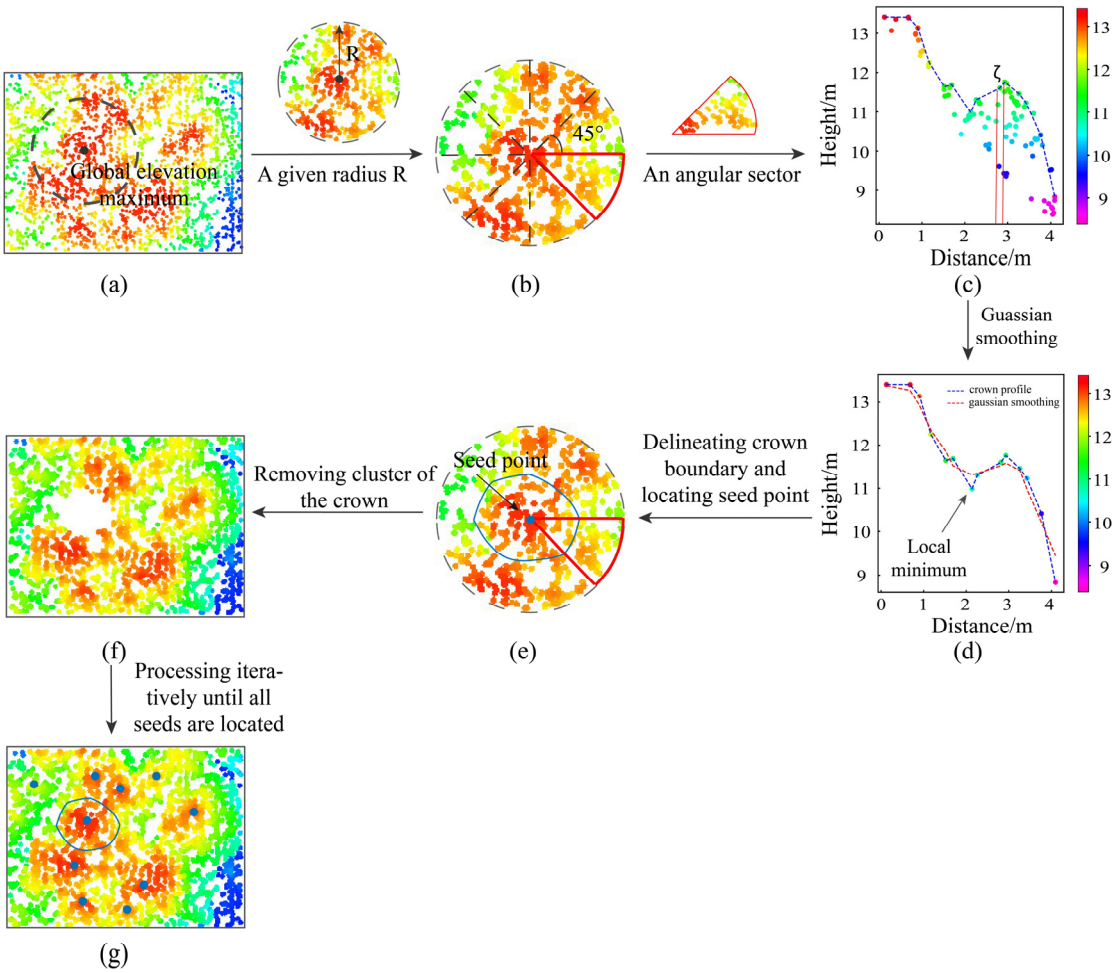

Figure 6. Workflow of extraction of seed points. Different colors represent different elevations. (**a**) Searching for the point clouds centered on the global elevation maximum; (**b**) Dividing the point clouds into eight sectors; (**c**) Modeling the Distance-Height relationship, (**d**) Gaussian smoothing; (**e**) Locating seed point; (**f**) The remaining point clouds; (**g**) The results of seed point detection.

The crown surface points were initially projected onto the XOY plane. The global elevation maximum, denoted as $p_c(x_c, y_c, z_c)$ (i.e., the tallest treetop), was taken as the center for the searching of points within a given radius R (where R is greater than the maximum crown radius). Subsequently, the searched points were categorized into eight

sectors at 45° intervals, as illustrated in Figure 6b. The point clouds $P_R^n = \{p_i^n\}_{i=1}^M$ (where M represents the number of points within the radius R and n denotes the sector number, n = 1, 2, . . ., 8) corresponding to each sector were calculated as follows:

$$\alpha_n \in [2\pi(n-1)/N, 2\pi n/N] \tag{1}$$

where α_n represents the range of each angular sector and N represents the total number of angular sectors.

The LiDAR points within each angular sector were projected onto the XOY plane and the distance d_i^n from $p_i^n(x_i^n, y_i^n, z_i^n)$ to the center p_c (Equation (2)) was calculated to model the distance–height relationship. Thereafter, the horizontal axis was divided into m intervals of ζ (Equation (3)) and the maximum height value within each interval was retained, as shown in Figure 6c. To avoid the impact of valley points located between a stretched branch and the crown on the detection of crown boundary points, a Gaussian function was employed to smooth these points and fit them into a curve (Equation (4)). As the tree height decreases in all directions from the center, a valley forms between two adjacent trees. Therefore, the first local minimum of the curve can be considered as the crown boundary point within the angular sector, and its distance—denoted as d_m^n—is the crown radius of the angular sector, as shown in Figure 6d,e. The boundary points of eight angular sectors are sequentially detected, the crown radius in each direction is recorded and the point clouds within the crown radius are marked. The marked point clouds represent the tree crown with p_c as the center, where p_c is the seed point, as shown in Figure 6e. The process continues by detecting the highest point among unmarked LiDAR points and marking the crown points centered on this point using the above-mentioned method. Seed points can be extracted once all LiDAR points have been marked.

$$d_i^n = \sqrt{(x_i^n - x_c)^2 + (y_i^n - y_c)^2} \tag{2}$$

$$m = \lceil (d_{max}^n - d_{min}^n)/\zeta \rceil \tag{3}$$

$$f(Z) = exp\left(-(Z-\mu)^2/\sigma^2\right)/\sigma\sqrt{2\pi},\ Z = \{z_k\}_{k=1}^m \tag{4}$$

where d_{max}^n and d_{min}^n represent the maximum and minimum distance values between the LiDAR points and center in an angular sector, respectively. $f(Z)$ represents the elevation value after Gaussian smoothing. Z and μ represent the real elevation value and the central position of the points, respectively. z_k represents the elevation value of the highest point in the kth interval. σ represents the standard deviation, which determines the smoothness of the curve.

3.1.3. Elimination of False Seed Points

The growth condition of all the trees in the forest differs, and the parameters for the Gaussian function must consider the overall situation. Therefore, the dips between some stretched branches and the crown cannot be ignored by Gaussian smoothing and are consequently recognized as crown boundaries (Figure 7a). As a result, the calculated crown radius is smaller than the actual value. The tops of stretched branches are mistakenly identified as seed points, leading to a decrease in the accuracy of seed point detection. When the smoothness parameter of the Gaussian function is set to a high value, it reduces the detection of some false seed points but may result in the omission of some correct ones.

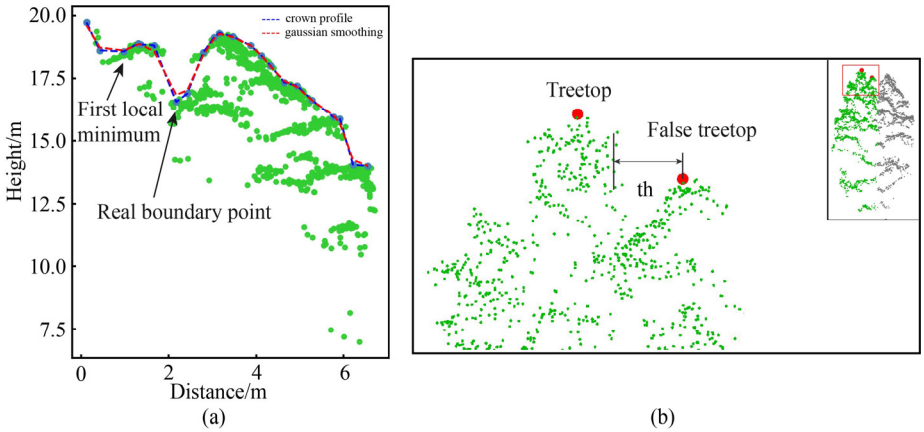

Figure 7. Detection process of false treetops: (**a**) distance–height relationship of tree in angular sector, (**b**) diagram of real and false treetop.

Given that the crown point clouds radiate outward from the center with decreasing height, there must be some higher points beyond the interval of the false seed points and the crown [8]. Consequently, a threshold (th) was set to remove the false seed points and improve the accuracy of seed point detection. Specifically, the seed point is used as the center and th as the radius to determine the presence of points that are higher than the seed point in the neighboring point cloud; if such a point exists, the seed point must be false (Figure 7b). It should be noted that the threshold (th) must be smaller than the crown radius and greater than the interval ζ.

3.1.4. Individual Tree Segmentation Based on Seed Points

In this study, a top-bottom region growing algorithm [33] was used to segment individual trees from normalized forest point clouds based on the detected seed points. The region growing algorithm segments trees based on distance thresholding, minimum spacing rules and the horizontal profile of tree shapes, where the distance threshold is approximately equal to the crown radius. The detailed process is as follows. The first step is to determine whether the horizontal distance between the neighboring point and the seed point falls within the distance threshold. If so, the point is considered as a portion of the tree, in accordance with the minimum spacing rule. The projected shape of the tree in the horizontal plane, along with the distribution of points, is subsequently utilized to determine whether the tree is over-segmented. If it is, the classification results are improved to reduce the over-segmentation error. Finally, the individual trees in the forest are segmented iteratively from top to bottom.

3.2. Extraction of Geometric Features

Crown structural parameters not only serve as indicators of individual tree growth but also provide essential data for the monitoring of forest dynamics. A schematic diagram for the estimation of crown structural parameters is shown in Figure 8, which comprises the tree height (Figure 8c), crown diameter (Figure 8a) and crown projection area (Figure 8b).

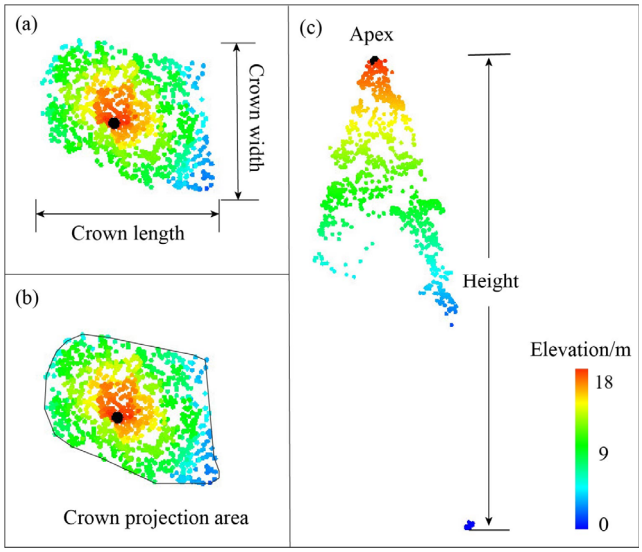

Figure 8. Estimation of crown structural parameters. (**a**) Crown diameter; (**b**) Crown projection area; (**c**) Tree height.

3.2.1. Tree Height

The tree height is defined as the vertical distance between the treetop and the ground-level point in the z-direction [46]. The elevation value of the treetop is equivalent to the tree height, as the height of the normalized ground point is zero, as shown in Figure 8c. In this study, a treetop is regarded as a seed point, and, as such, the elevation (z-value) of this seed point represents the tree height.

3.2.2. Crown Diameter

The crown diameter is calculated as the average of measurements taken in two perpendicular directions: the crown length and crown width [47]. As depicted in Figure 8a, the crown length is defined as the distance between the maximum and minimum values in the east–west direction, and the crown width is determined as the distance between the maximum and minimum values in the north–south direction. The average of these measurements in both the east–west and north–south directions yields the crown diameter.

3.2.3. Crown Projection Area

The crown projection area is defined as the area of the crown projected onto the XOY plane, as shown in Figure 8b. Regular shapes often do not represent the actual shape of tree crowns, so the convex hull method was used to calculate the projection area of crowns in this study. This method gradually searches the outermost points in the projected LiDAR points initially. Subsequently, these points are connected to form a convex polygon. Finally, the crown projection area is determined by calculating the area of the convex polygon using Equation (5), where n represents the number of vertexes of the convex polygon.

$$S = 1/2 * \sum_{i=1}^{n} (x_i * y_{i+1} - x_{i+1} * y_i) \quad (5)$$

3.3. Accuracy Assessment

The accuracy of the experimental results was evaluated from three main aspects: seed point detection, individual tree segmentation and the extraction of crown structural parameters.

The results of the detected seed points were compared to the measured data, and the recall (R), precision (P) and F1-score (F1) (Equations (6)–(8)) were calculated to validate the accuracy of the seed point detection.

$$R = TP/(TP + FN) \times 100\% \quad (6)$$

$$P = TP/(TP + FP) \times 100\% \quad (7)$$

$$F1 = 2 \times (R \times P)/(R + P) \quad (8)$$

where true positive (TP), false negative (FN) and false positive (FP) represent the number of correctly identified seed points, missed seed points and incorrectly identified seed points, respectively.

The trees extracted by the proposed algorithm were considered as the detected data, while the manually extracted individual trees from the point clouds were taken as the reference data. The accuracy of individual tree segmentation was evaluated in terms of the accuracy rate (AR), commission error (CE) and omission error (OE) using Equations (9)–(11). Trees that have an intersection of union (IoU) with the reference trees exceeding 50% are regarded as correctly segmented trees (C) (Equation (12)) [48,49]. Over-segmentation (O) means that a reference tree is segmented into multiple trees, whereas under-segmentation (U) means that two or more reference trees are taken as one tree.

$$AR = N_C/N_{REF} \times 100\% \quad (9)$$

$$CE = N_O/N_{REF} \times 100\% \quad (10)$$

$$OE = N_U/N_{REF} \times 100\% \quad (11)$$

$$IoU = (P_{det} \cap P_{ref})/(P_{det} \cup P_{ref}) \times 100\% \quad (12)$$

where P_{det} and P_{ref} are the point cloud sets of the detected tree and reference tree; N_{REF} represents the number of the reference trees; and N_C, N_O and N_U represent the number of correctly segmented, over-segmented and under-segmented trees, respectively.

The crown structural parameters calculated in this study were the tree height, crown diameter and crown projection area. The coefficient of determination (R^2), root mean square error (RMSE) and relative RMSE (rRMSE) were used to evaluate the accuracy of these parameters, as given in Equations (13)–(15).

$$R^2 = 1 - \sum(y_i - \hat{y}_i)^2/\sum(y_i - \overline{y}_i)^2 \quad (13)$$

$$RMSE = \sqrt{\sum(y_i - \hat{y}_i)^2/n} \quad (14)$$

$$rRMSE = RMSE/\overline{y}_i \times 100\% \quad (15)$$

where y_i and $\hat{y}_i$ are the measured value and the estimated value of the crown parameters, and $\overline{y}_i$ is the average of the measured values.

4. Results

4.1. Results of Extracted Canopy Surface

In this study, the interval of the Y-axis of plots 1 to 4 was set to 0.05 m, 0.1 m, 0.1 m and 0.1 m, respectively. Figure 9 depicts the original point clouds and extracted crown surface points in the four plots, with (a1)–(d1) corresponding to plots 1 to 4 in Figure 1. The crown surface points obtained from multiple angles were merged to preserve the shape and spatial characteristics of the forest as accurately as possible. The extracted crown surface points significantly improved the efficiency of seed point detection, leading to an average reduction of 90.8% in the point cloud density without sacrificing the canopy detail.

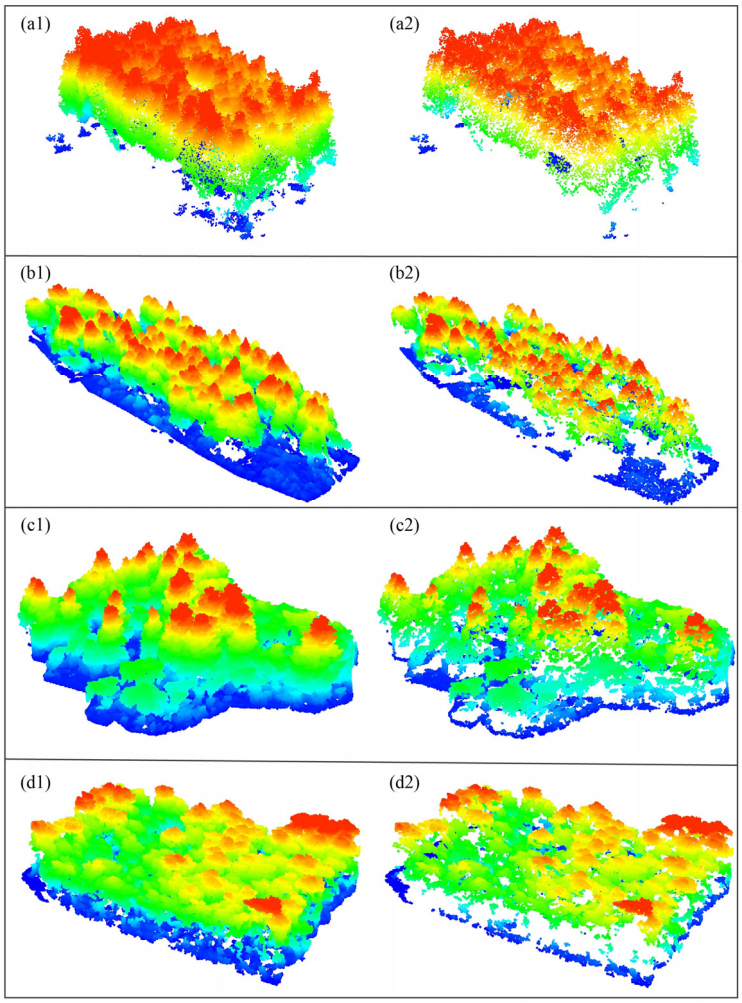

Figure 9. Original point clouds and crown surface points of four plots. Different colors represent different elevations. (**a1–d1**) are original point clouds of plots 1 to 4 and (**a2–d2**) are crown surface points of plots 1 to 4.

4.2. Results of Detected Seed Points

The search radius (R) for crown surface points should be greater than the maximum crown radius [41]. As a result, the R for plots 1 to 4 was set to 3.5 m, 3.5 m, 7.5 m and 6.0 m, respectively, taking into account the measured crown diameters in each plot. In this study, 11 sets of parameters were set for each plot to analyze the effect of the interval (ζ) on seed point detection via the analysis of the planting density and crown size, and 0.05 m, 0.5 m, 0.6 m and 0.5 m were selected for the extraction of the maximum height point within the interval ζ in the distance–height relationship for each angular sector, respectively. Subsequently, these points were smoothed and fitted to a curve using the Gaussian function.

To analyze the effect of the Gaussian smoothing parameter (σ) on seed point detection, ten sets of parameters were set up for each plot based on the forest type. The optimal values of σ were determined as 0.3, 0.5, 0.5 and 0.5 for plots 1 to 4, respectively. The first local minimum of the smoothed curve was regarded as the crown boundary point within each angular sector, and then the crown boundary was delineated to obtain seed points. A threshold (th) was set to eliminate the interference from some stretched branches on seed point detection. The value should be smaller than the crown radius (the average crown radii of plots 1 to 4 are 0.885 m, 2.318 m, 3.550 m and 2.364 m, respectively) and larger than the interval ζ. As a result, the th values were set to 0.5 m, 0.8 m, 1.2 m and 0.5 m for plots 1 to 4, respectively. Figure 10 depicts the results of seed point detection in the four

plots. As can be seen in the figure, the majority of the seed points were detected, and their positions mostly corresponded to the locations of treetops, with plot 1 showing the best detection results. Table 4 shows the accuracy of seed point detection for the four plots. Plots 1 and 2 are both coniferous forests, while plots 3 and 4 are mixed and broadleaf forests, respectively. As shown in the table, the F1 of seed point detection for plots 1 to 4 was 0.94, 0.90, 0.86 and 0.84, respectively; the R was 91.6%, 89.2%, 88.2% and 82.2%, respectively; and the P was 95.9%, 91.2%, 84.2% and 85.5%, respectively. In the four plots, the accuracy of seed point detection was highest in the coniferous forest—particularly in the plot with flat terrain, where the R, P and F1 were higher than those in the coniferous forest with sloping terrain. The R and F1 for the seed point detection were higher in the mixed forest compared to the broadleaf forest, although the P was slightly lower. This phenomenon can be attributed to the diverse tree species and significant presence of taller coniferous trees with stretched branches in plot 3. As a result, a substantial number of branch tops were mistakenly identified as seed points, leading to decreased precision.

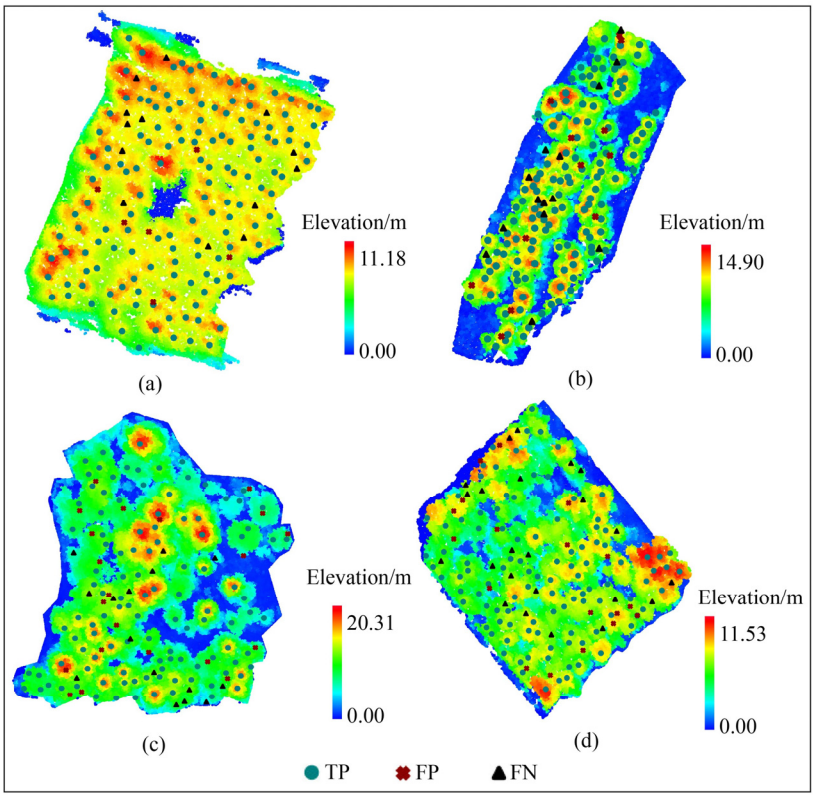

Figure 10. Results of seed point detection of plots 1 to 4. TP represents correct seed points; FN represents missed seed points; and FP represents false seed points. (**a**–**d**) are plots 1 to 4, respectively.

Table 4. Accuracy of seed point detection of plots 1 to 4.

Plot	Detected Seed Point	TP	FN	FP	R	P	F1
P1	147	141	13	6	91.6%	95.9%	0.94
P2	136	124	15	12	89.2%	91.2%	0.90
P3	133	112	15	21	88.2%	84.2%	0.86
P4	124	106	23	18	82.2%	85.5%	0.84

4.3. Results of Individual Tree Segmentation

The region growing algorithm was used to segment individual trees within the four plots based on the detected seed points, and the results are shown in Figure 11. The majority of individual trees in the four plots with clear treetops and crown boundaries

were successfully segmented. The accuracy of individual tree segmentation was evaluated using AR, CE and OE.

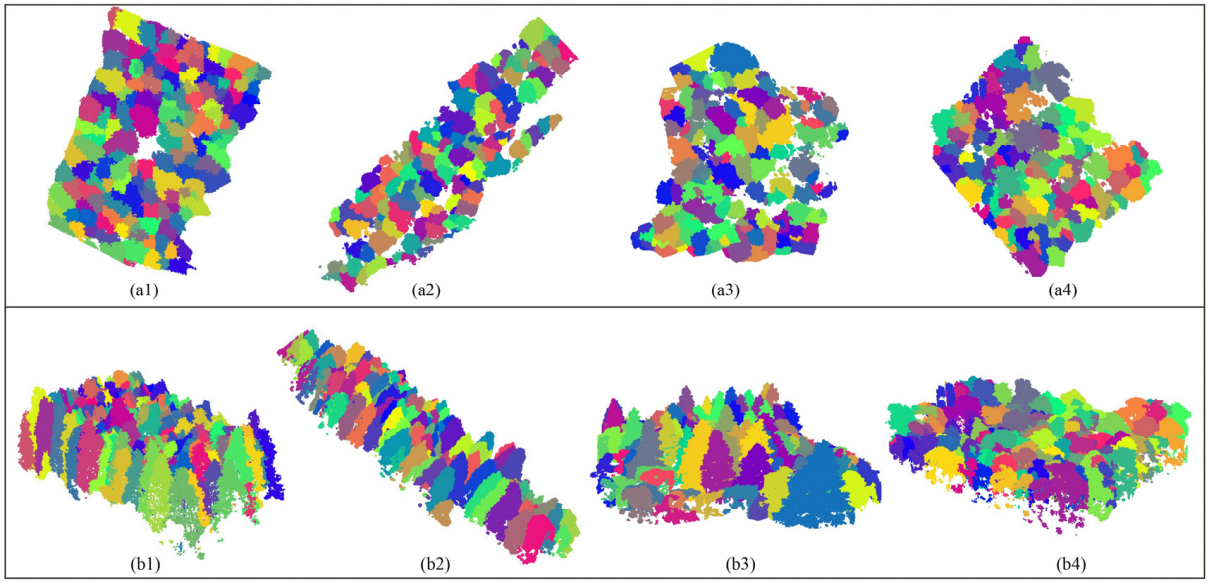

Figure 11. Results of individual tree segmentation of four plots. Different colors represent different trees. (**a1**–**a4**) are top views of individual tree segmentation for plots 1 to 4, respectively. (**b1**–**b4**) are side views of individual tree segmentation for plots 1 to 4, respectively.

The results of individual tree segmentation are shown in Table 5. There were 549 trees in the four plots in total, and our method correctly segmented 431 trees, over-segmented 52 trees and under-segmented 66 trees. For all plots, the overall AR, CE and OE were 78.5%, 9.5% and 12.0%, respectively. The AR for plots 1 to 4 was 87.7%, 80.6%, 73.2% and 70.5%, respectively; the CE was 3.9%, 8.6%, 14.9% and 11.6%, respectively; and the OE was 8.4%, 10.8%, 11.8% and 17.8%, respectively. The AR of individual tree segmentation decreased in descending order for coniferous, mixed and broadleaf forest, and the coniferous forest on flat terrain yielded better results than that on sloping terrain. It was apparent that the CE was higher in the mixed forest than in the broadleaf forest, because a large number of stretched branch tops of tall conifers were misidentified as seed points, resulting in over-segmentation.

Table 5. Results of individual tree segmentation with our method for four plots.

Plot	Reference Tree	Correctly Segmented	Over-Segmented	Under-Segmented	AR	CE	OE
P1	154	135	6	13	87.7%	3.9%	8.4%
P2	139	112	12	15	80.6%	8.6%	10.8%
P3	127	93	19	15	73.2%	14.9%	11.8%
P4	129	91	15	23	70.5%	11.6%	17.8%
Total	549	431	52	66	78.5%	9.5%	12.0%

4.4. Estimation of Crown Structural Parameters

For the correctly segmented trees in plots 1 to 4, the parameters of tree height, CD and CPA were estimated. Linear regression was used to analyze the relationship between the estimated and measured parameters, while the R^2, RMSE and rRMSE were calculated to evaluate the accuracy of the estimated parameters for plots 1 to 4. Figures 12–14 show the estimated accuracy for the tree height, CD and CPA, respectively. As shown in Figure 12, the R^2 was nearly equal to 1 for the four plots, and most of the estimated tree heights were equal to the measured values, indicating the high accuracy of the estimated tree height

and the locations of seed points. Figure 13 shows the results of CD estimation in the four plots: the R^2 was higher than 0.80; the RMSE for plots 1 to 4 was 0.21 m, 0.28 m, 0.83 m and 0.78 m, respectively; and the rRMSE was 11.88%, 6.19%, 12.10% and 16.74%, respectively. The coniferous forest yielded better results than the mixed forest and the broadleaf forest. Additionally, the coniferous forest with sloping terrain yielded better results than that with flat terrain, which was caused by the high stem density (5540 plants/ha) and closely spaced trees with overlapping branches. It can be seen from Figure 14 that the R^2 for the estimated CPA was higher than 0.80 for the four plots; the RMSE for plots 1 to 4 was 0.51 m^2, 2.18 m^2, 8.66 m^2 and 6.52 m^2, respectively; and the rRMSE for these same plots was 22.13%, 13.48%, 23.42% and 39.51%, respectively. The accuracy of the estimated CPA was highest for the coniferous forest with sloping terrain, lowest in the broadleaf forest and generally intermediate in the coniferous forest with flat terrain and the mixed forest.

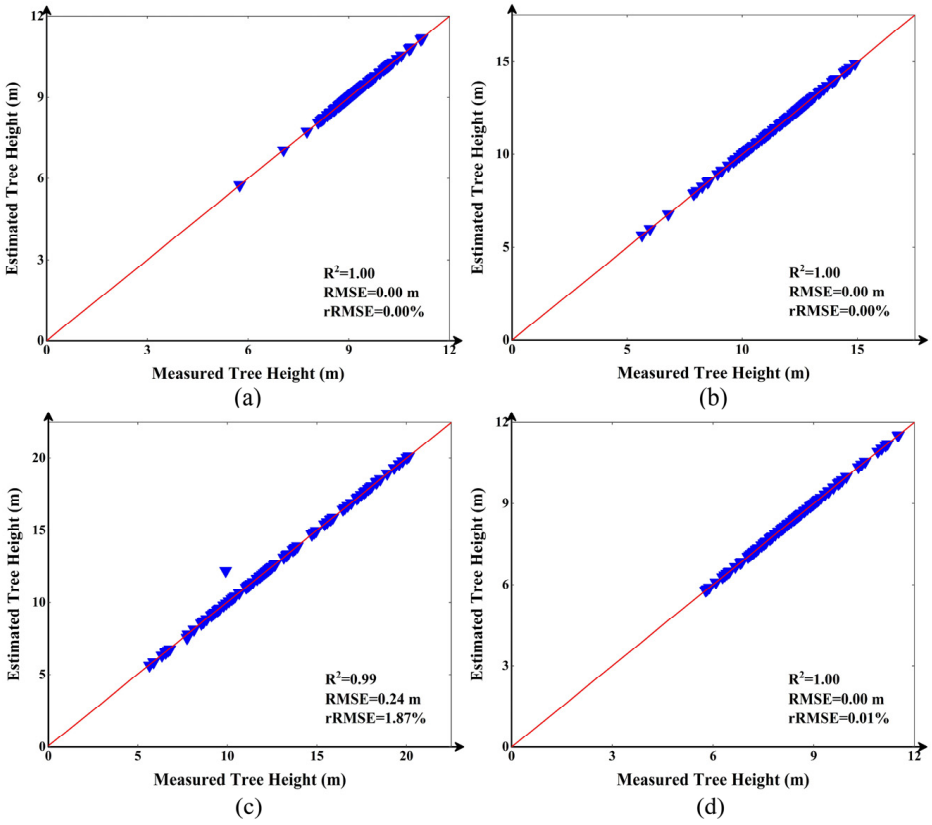

Figure 12. Relationship between estimated and measured tree height. The red line is 1:1 control line. (**a**–**d**) are plots 1 to 4, respectively.

In summary, the coniferous forest with sloping terrain performed the best due to its low planting density and well-defined crown boundaries, followed by the coniferous forest with flat terrain and the mixed forest, and lastly the broadleaf forest. It can be concluded that the stem density and canopy complexity exerted a noticeable influence on the accuracy of the estimated CD and CPA of individual trees. Moreover, the proposed method demonstrated a high level of accuracy in estimating the tree height, closely approximating the measured values.

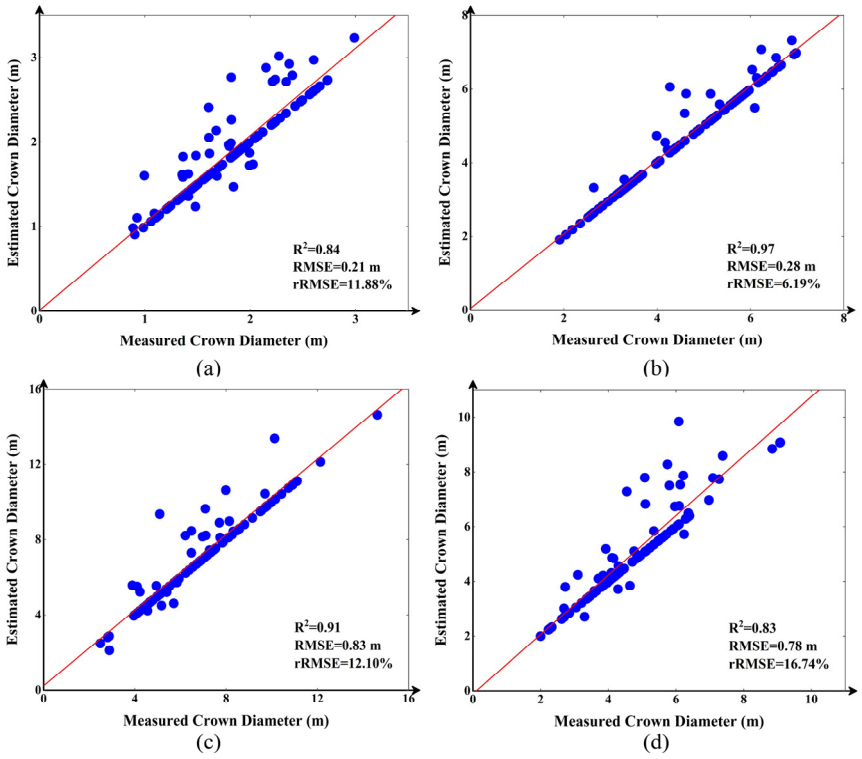

Figure 13. Relationship between estimated and measured crown diameter. The red line is 1:1 control line. (**a**–**d**) are plots 1 to 4, respectively.

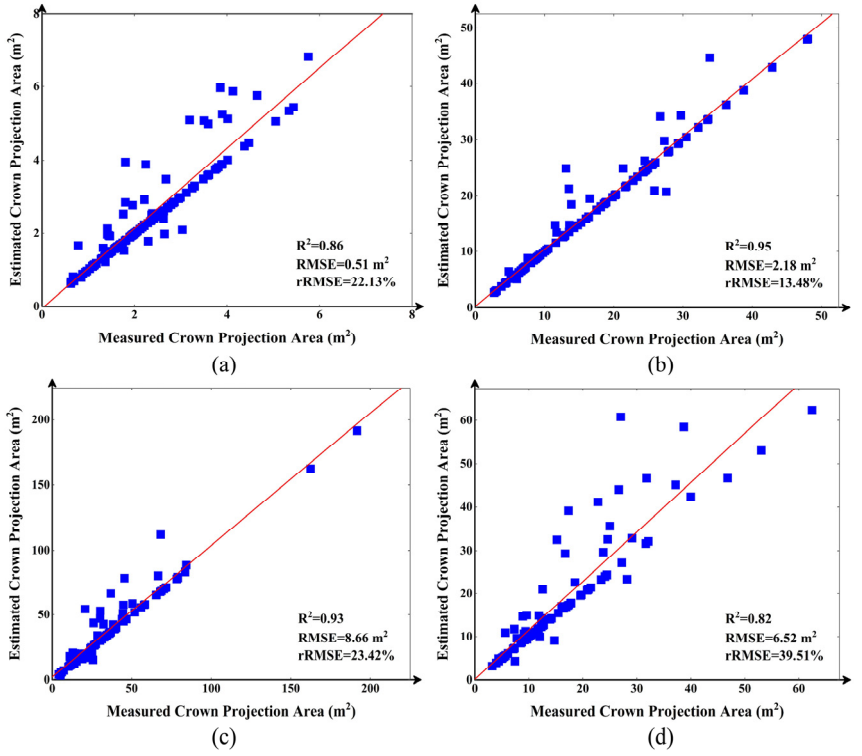

Figure 14. Relationship between estimated and measured crown projection area. The red line is 1:1 control line. (**a**–**d**) are plots 1 to 4, respectively.

5. Discussion

5.1. Factors Affecting Precision

5.1.1. Determination of the Interval of Y-Axis

The planting density and crown size of each plot were taken into account to determine the Y-axis interval for different plots. For plots 1 to 4, the planting densities were 5540 plants/ha, 464 plants/ha, 260 plants/ha and 612 plants/ha, accompanied by average crown diameters of 1.770 m, 4.635 m, 7.101 m and 4.727 m, respectively. Consequently, the intervals of the Y-axis of plots 1 to 4 were set to 0.05 m, 0.1 m, 0.1 m and 0.1 m, respectively.

5.1.2. Effect of Interval ζ

In this study, 11 sets of parameters were set up for each plot to analyze the effect of ζ on seed point detection based on the forest type. To generate a more detailed crown profile, the settings for the range of ζ and varied intervals of plot 1 had to be smaller than those of the other three plots. This was because the planting density of plot 1 was greater than nine times that of the other plots and its average crown diameter was approximately one third of that of the other plots (Table 2). Therefore, ζ was set to vary from 0 m to 0.5 m at 0.05 m intervals for plot 1, and from 0 m to 1.0 m at 0.1 m intervals for the other plots, respectively.

Figure 15 shows the accuracy of seed point detection in the four plots for different ζ. For plot 1, the results for seed point detection at ζ of 0 m and 0.05 m were identical. However, as ζ increased beyond 0.05 m, P increased, while both R and F1 decreased (Figure 15a). Therefore, an optimal interval of 0.05 m was selected for plot 1, with computational efficiency taken into consideration. For plot 2, as ζ increased, the P of the seed point detection gradually increased, while R exhibited a declining trend. R reached its peak at ζ of 0.3 m and 0.5 m, and F1 performed best at ζ of 0.5 m (Figure 15b). For plot 3, the overall trend shows that the P of seed point detection increased as ζ increased, while R decreased, and F1 reached its maximum value at ζ of 0.6 m (Figure 15c). For plot 4, the P of seed point detection generally increased with increasing ζ—an especially sharp increase was observed within the 0–0.5 m range, while R decreased and F1 was highest at ζ of 0.5 m (Figure 15d). In conclusion, the accuracy of seed point detection for plots 1 to 4 was found to be optimal at ζ of 0.05 m, 0.5 m, 0.6 m and 0.5 m, respectively.

5.1.3. Effect of Gaussian Smoothing Parameter σ

In the study, ten sets of parameters were established for each plot to analyze the impact of the Gaussian smoothing parameter σ on seed point detection. For each plot, σ was set to range from 0.1 to 1.0 at intervals of 0.1. Figure 16 depicts the results of seed point detection for the four plots under different σ. In plot 1, σ had a minor effect on seed point detection. The P of seed point detection consistently increased as σ increased, while R decreased, and the F1 of seed point detection was optimal when σ was 0.3 (Figure 16a). In plot 2, the P of seed point detection increased with higher σ, while R decreased, and F1 was optimal at σ = 0.5 (Figure 16b). In plot 3, the P of seed point detection increased with higher σ within 0.2–0.7 and reached its peak at σ = 0.7. R showed a declining trend and reached its peak when σ was 0.5, while F1 reached its peak at σ = 0.5 (Figure 16c). In plot 4, the P of seed point detection increased as σ increased, while R peaked at σ = 0.3 and then declined. F1 was optimal when σ was 0.5. In conclusion, the accuracy of seed point detection was optimized at σ = 0.3 for plot 1 and at σ = 0.5 for the other plots. The results show that σ influenced the accuracy of seed point detection differently depending on the forest type. Specifically, seed point detection in the coniferous forest with flat terrain and uniform growth was less affected by σ.

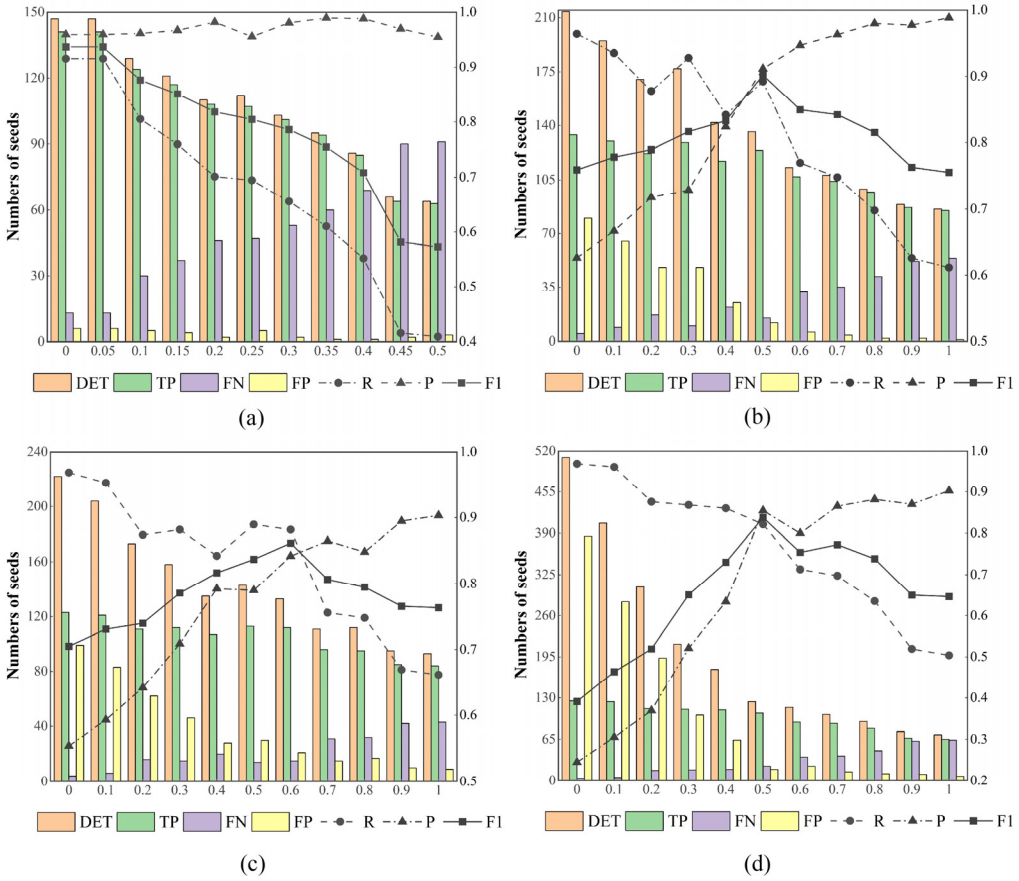

Figure 15. Results of seed point detection using different intervals. (**a**–**d**) are plots 1 to 4, respectively.

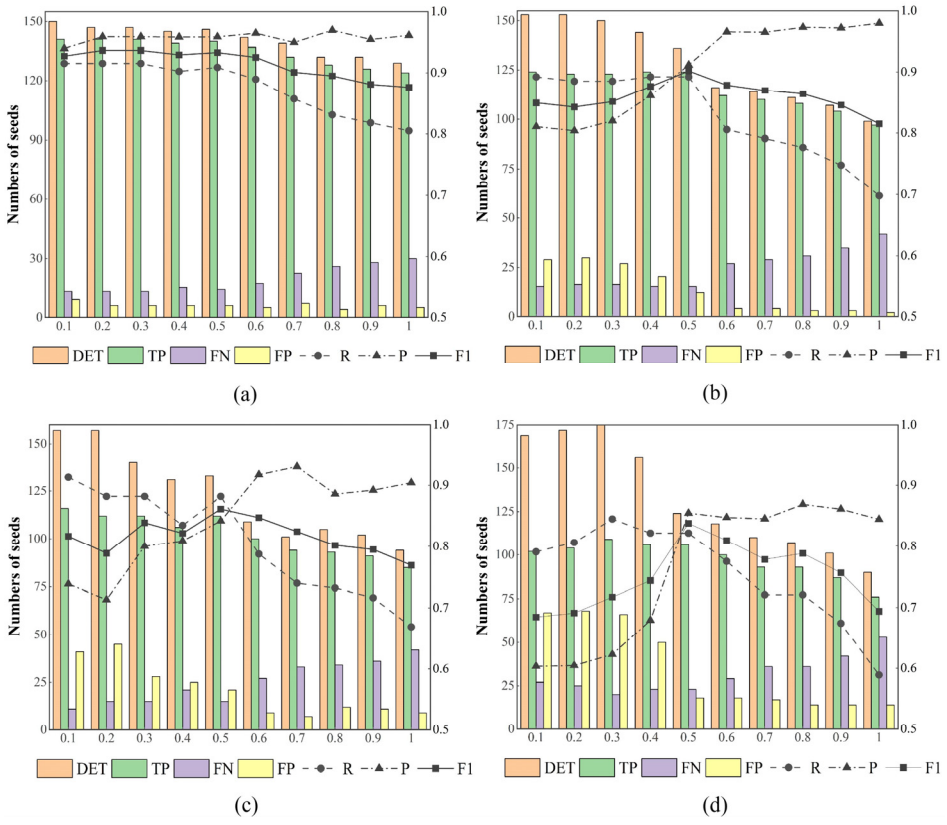

Figure 16. Results of seed point detection using different σ. (**a**–**d**) are plots 1 to 4, respectively.

5.2. Comparison with Existing Methods

5.2.1. Seed Point Detection

In this study, the proposed method was compared with the local maximum method (LM) and the CHM-based method. Table 6 shows the results of seed point detection using the three methods with the four plots.

Table 6. Comparisons among different methods.

Plot	P1			P2			P3			P4		
Method	**LM**	**CHM**	**Proposed**	**LM**	**CHM**	**Proposed**	**LM**	**CHM**	**Proposed**	**LM**	**CHM**	**Proposed**
Detected Seed Points	160	140	147	126	134	136	126	118	133	114	120	124
TP	133	130	141	114	121	124	104	106	112	95	104	106
FN	11	24	13	25	18	15	23	21	15	34	25	23
FP	17	10	6	12	13	12	22	12	21	19	16	18
R	90.4%	84.4%	91.6%	82.0%	87.1%	89.2%	81.9%	83.4%	88.2%	73.6%	80.6%	82.2%
P	83.1%	92.9%	95.9%	91.2%	90.3%	91.2%	82.5%	89.8%	84.2%	83.3%	86.7%	85.5%
F1	0.86	0.88	0.94	0.86	0.89	0.90	0.82	0.86	0.86	0.78	0.84	0.84

The proposed method performed the best in seed point detection, with R, P and F1 ranging from 82.2% to 91.6%, 84.2% to 95.9% and 0.84 to 0.94, respectively. This was followed by the CHM-based method, with R, P and F1 ranging from 80.6% to 87.1%, 86.7% to 92.9% and 0.84 to 0.89, respectively. The LM method exhibited the lowest accuracy, with R, P and F1 within the range of 73.6% to 90.4%, 82.5% to 91.2% and 0.78 to 0.86, respectively. The LM and CHM-based method performed well in the coniferous forest, but the R was lower due to the irregular crown shape, especially in the mixed forest and broadleaf forest. This is because these two methods are highly dependent on the window size. To enhance the precision of the seed points, the window size was adjusted to accommodate larger crowns, resulting in the tops of smaller trees being ignored.

Compared to the other two methods, our proposed method has shown improvements in R and P and produced a greater number of correct seed points. Note that our method did not achieve optimal P values in plots 3 and 4, which was likely due to the heavy reliance of our method on the crown geometry. The indistinct treetops and crown boundaries of broadleaves, along with their elongated branches, have negative impacts on seed point detection, which will be a topic for future work.

5.2.2. Individual Tree Segmentation

In order to validate the effectiveness of our proposed method, a comparative test was carried out with the point cloud segmentation method (PCS). Table 7 and Figure 17 show the results of individual tree segmentation for the four plots.

Table 7. Results of individual tree segmentation with PCS.

Plot	Reference Tree	Correctly Segmented	Over-Segmented	Under-Segmented	AR	CE	OE
P1	154	126	10	18	81.8%	6.5%	11.7%
P2	139	104	15	20	74.8%	10.8%	14.4%
P3	127	85	19	23	67.0%	14.9%	18.1%
P4	129	79	23	27	61.2%	17.8%	20.9%
Total	549	394	67	88	71.8%	12.2%	16.0%

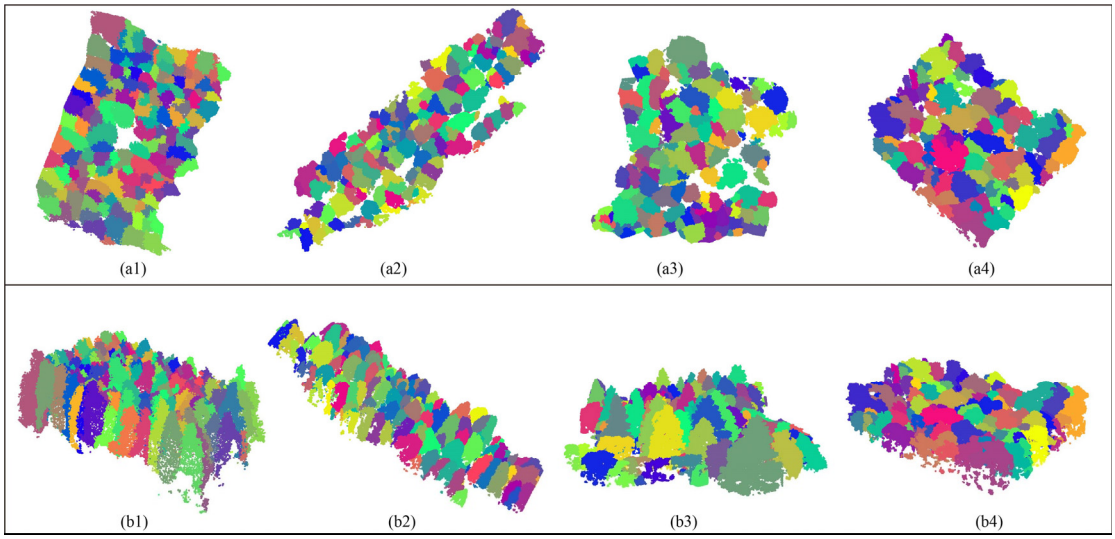

Figure 17. Results of individual tree segmentation with PCS. Different colors represent different trees. (**a1**–**a4**) are top views of individual tree segmentation for plots 1 to 4, respectively. (**b1**–**b4**) are side views of individual tree segmentation for plots 1 to 4, respectively.

As shown in Figure 17, PCS performed well in coniferous forests but worst in mixed forest and broadleaf forest, with large over-segmentation and under-segmentation. Accordingly, as seen in Table 7, the overall AR, CE and OE were 71.8%, 12.4% and 16.2%, respectively. The overall accuracy of PCS was slightly lower than that of our proposed method. As shown in Figure 18, PCS suffered from over-segmentation and under-segmentation, indicating that the segmentation results were unsatisfactory. This is because trees in natural forests vary in height and are interspersed with each other, which might lead to lower trees being mistakenly categorized to a part of the neighboring large trees.

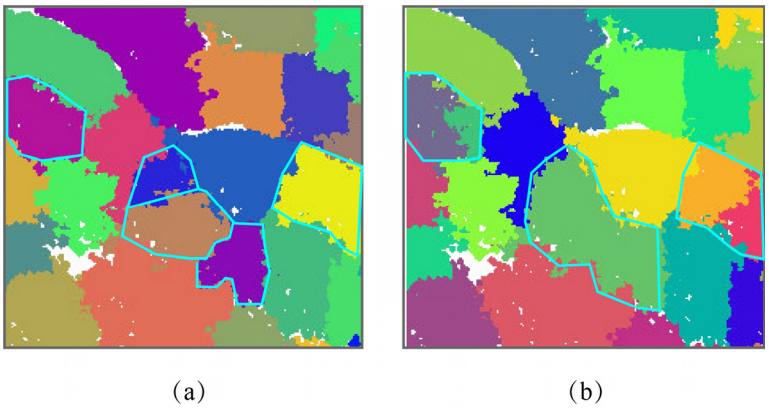

Figure 18. An example of segmentation results in plot 2. Different colors represent different trees. The blue box represents a single tree. (**a**) Our proposed method; (**b**) PCS.

Compared with PCS, our approach significantly improved the overall accuracy of individual tree segmentation, with an increase of 6.7% in AR and decreases of 2.7% and 4.0% in CE and OE, respectively. For plots 1 to 4, AR exhibited an improvement ranging from 5.8% to 9.3%, with CE being reduced between 0% and 6.2% and OE decreasing within the range of 3.1% to 6.2%. It is clear that our method showed a more pronounced improvement in accuracy for the broadleaf forest.

5.3. Limitations and Prospects

The accuracy of seed point detection affects the accuracy of individual tree segmentation, which is a prerequisite in obtaining the details of individual trees and can provide

essential data for forest protection and management. To detect seed points with high precision, we have presented an individual tree segmentation method based on seed points detected by an adaptive crown shaped algorithm. This method directly searches the seed points on the crown surface points, which improves the efficiency of seed point detection while preserving the shape characteristics and spatial relationships of the crowns. Furthermore, the number of false seed points is minimized based on the marked crown boundary and distance thresholds between trees, which reduces the interference of false treetops in seed point detection. In this study, the proposed method performed well in coniferous forest, mixed forest and broadleaf forest, with an overall AR of 78.5%. Our method takes into consideration the crown shape and can be applicable to forests with different forest types and topographies, allowing for high-precision seed point detection. Individual tree segmentation based on this method contributes to detailed forest resource surveys, providing precise data for forest research.

However, the proposed method retains some shortcomings: (1) the proposed method for seed point detection has high F1-scores, but the omission errors can be relatively high—future research could focus on how to improve the algorithm, through reducing the number of missed seed points; (2) this method lacks validation in complex forests with denser understory vegetation, which will be applied in the future to verify its applicability to forests with abundant understory vegetation.

In order to improve the accuracy of our method, the following two aspects will be focused on in our future work: (1) we will consider integrating point cloud data with 2D imagery data, combining the strengths of these two data types, to achieve high accuracy in individual tree segmentation and obtain high-precision crown parameters; (2) machine learning methods are able to automatically learn features from sample data and can be applied to various scenarios; therefore, deep learning methods (i.e., PointNet, PointNet ++) will be implemented to segment individual trees in the future.

6. Conclusions

This study presented an individual tree segmentation method based on seed points detected by an adaptive crown shaped algorithm. It realized seed point detection and individual tree segmentation in four experimental plots with varied forest types and topographies. The results showed the following.

(1) The proposed method performed well in seed point detection and individual tree segmentation. The crown structure and distance between trees were considered in the adaptive crown shaped algorithm to detect seed points accurately. (2) The tree height, crown diameter and crown projection area were extracted based on the segmented individual trees. Compared with the measured data, the estimated crown parameters showed high accuracy, especially in the natural coniferous forest. (3) Compared with the other algorithms for seed point detection and individual tree segmentation, our method exhibited superior performance across the four plots, with significant improvements in the overall accuracy.

The proposed method was applied to forests of various tree species with varying terrains, demonstrating its capability to obtain seed points and segment individual trees with high accuracy. This lays the foundation for the accurate estimation of forest structural parameters, thereby significantly contributing to the improved accuracy of forest inventory.

Author Contributions: Conceptualization, J.Y., L.L. and Z.L.; methodology, J.Y. and L.L.; software, J.Y.; validation, J.Y. and L.L.; formal analysis, J.Y. and L.L.; investigation, J.Y. and L.L.; data curation, J.Y.; writing—original draft preparation, J.Y.; writing—review and editing, L.L. and Z.L.; visualization, J.Y. and L.L.; supervision, L.L. and Z.L.; resources, Z.L.; project administration, Z.L.; funding acquisition, L.L. and Z.L. All authors have read and agreed to the published version of the manuscript.

Funding: This work was supported by the Shaanxi Province Science and Technology Innovation Team (2021TD-51), the Shaanxi Province Geoscience Big Data and Geohazard Prevention Innovation Team (2022), the European Space Agency through the ESA-MOST DRAGON-5 Project (59339) and the Fundamental Research Funds for the Central Universities, Chang'an University (300102260301, 300102262902, 300102262712).

Data Availability Statement: Data are contained within the article.

Acknowledgments: The authors would like to thank the editors and reviewers for their advice.

Conflicts of Interest: The authors declare no conflicts of interest.

References

1. Li, Z.; Liu, Q.; Pang, Y. Review on forest parameters inversion using LiDAR. *J. Remote Sens.* **2016**, *20*, 1138–1150.
2. Jaskierniak, D.; Lucieer, A.; Kuczera, G.; Turner, D.; Lane, P.N.J.; Benyon, R.G.; Haydon, S. Individual tree detection and crown delineation from Unmanned Aircraft System (UAS) LiDAR in structurally complex mixed species eucalypt forests. *ISPRS J. Photogramm. Remote Sens.* **2021**, *171*, 171–187. [CrossRef]
3. Ferraz, A.; Bretar, F.; Jacquemoud, S.; Gonçalves, G.; Pereira, L.; Tomé, M.; Soares, P. 3-D mapping of a multi-layered mediterranean forest using ALS data. *Remote Sens. Environ.* **2012**, *121*, 210–223. [CrossRef]
4. Hao, Y.; Widagdo, F.R.A.; Liu, X.; Liu, Y.; Dong, L.; Li, F. A hierarchical region-merging algorithm for 3-D segmentation of individual trees using UAV-LiDAR point clouds. *IEEE Trans. Geosci. Remote Sens.* **2022**, *60*, 5701416. [CrossRef]
5. Koch, B.; Heyder, U.; Weinacker, H. Detection of individual tree crowns in airborne lidar data. *Photogramm. Eng. Remote Sens.* **2006**, *72*, 357–363. [CrossRef]
6. Ahmadi, S.A.; Ghorbanian, A.; Golparvar, F.; Mohammadzadeh, A.; Jamali, S. Individual tree detection from unmanned aerial vehicle (UAV) derived point cloud data in a mixed broadleaf forest using hierarchical graph approach. *Eur. J. Remote Sens.* **2022**, *55*, 520–539. [CrossRef]
7. Liang, X.; Pang, Y.; Chen, B. Accurate measurement of individual tree position based on DBH extraction of terrestrial laser scanning. *For. Res.* **2020**, *33*, 67–74.
8. Zhu, B.; Luo, H.; Jin, J.; Yue, C. Optimization of individual tree segmentation methods for high canopy density plantation based on UAV LiDAR. *Sci. Silvae Sin.* **2022**, *58*, 48–59.
9. Balsi, M.; Esposito, S.; Fallavollita, P.; Nardinocchi, C. Single-tree detection in high-density LiDAR data from UAV-based survey. *Eur. J. Remote Sens.* **2018**, *51*, 679–692. [CrossRef]
10. Xu, D.; Wang, H.; Xu, W.; Luan, Z.; Xu, X. LiDAR applications to estimate forest biomass at individual tree scale: Opportunities, challenges and future perspectives. *Forests* **2021**, *12*, 550. [CrossRef]
11. Liu, H.; Zhang, X.; Zhang, Y.; Zhu, Y.; Liu, H.; Wang, L. Review on individual tree detection based on airborne LiDAR. *Laser Optoelectron. Prog.* **2018**, *8*, 82805.
12. Lee, H.; Slatton, K.C.; Roth, B.E.; Cropper, W.P. Adaptive clustering of airborne LiDAR data to segment individual tree crowns in managed pine forests. *Int. J. Remote Sens.* **2010**, *31*, 117–139. [CrossRef]
13. Sun, Y.; Lin, W. Extraction of the parameters of single tree structure based on SFM algorithm. *J. Northwest For. Univ.* **2020**, *35*, 180–184+218. [CrossRef]
14. Wang, X.; Song, K.; Wang, Z.; Da, L.; Mokroš, M. Usage of Structure-from-Motion for urban forest inventory. *J. Southwest For. Univ. (Nat. Sci.)* **2021**, *41*, 139–148.
15. Huo, L.; Lindberg, E.; Holmgren, J. Towards low vegetation identification: A new method for tree crown segmentation from LiDAR data based on a symmetrical structure detection algorithm (SSD). *Remote Sens. Environ.* **2022**, *270*, 112857. [CrossRef]
16. Wu, X.; Shen, X.; Cao, L.; Wang, G.; Cao, F. Assessment of individual tree detection and canopy cover estimation using Unmanned Aerial Vehicle based Light Detection and Ranging (UAV-LiDAR) data in planted forests. *Remote Sens.* **2019**, *11*, 908. [CrossRef]
17. Yu, H.; Feng, S.; Shen, Y.; Liu, P. Research on single tree segmentation algorithm of UAV LiDAR plantation. *Laser Infrared* **2022**, *52*, 757–762. [CrossRef]
18. Itakura, K.; Miyatani, S.; Hosoi, F. Estimating tree structural parameters via automatic tree segmentation from LiDAR point cloud data. *IEEE J. Sel. Top. Appl. Earth Observ. Remote Sens.* **2022**, *15*, 555–564. [CrossRef]
19. Tang, F.; Ruan, Z.; Liu, X.; Zhang, Y. A new method of individual tree recognition based on airborne LiDAR data. *Remote Sens. Technol. Appl.* **2011**, *26*, 196–201.
20. Hamraz, H.; Contreras, M.A.; Zhang, J. Vertical stratification of forest canopy for segmentation of understory trees within small-footprint airborne LiDAR point clouds. *ISPRS J. Photogramm. Remote Sens.* **2017**, *130*, 385–392. [CrossRef]
21. Zhao, D.; Pang, Y.; Li, Z.; Liu, L. Isolating individual trees in a closed coniferous forest using small footprint LiDAR data. *Int. J. Remote Sens.* **2014**, *35*, 7199–7218. [CrossRef]
22. Geng, L.; Li, M.; Fan, W.; Wang, B. Individual tree structure parameters and effective crown of the stand extraction base on airborne LiDAR data. *Sci. Silvae Sin.* **2018**, *54*, 62–72.
23. Zhen, Z.; Quackenbush, L.J.; Stehman, S.V.; Zhang, L.J. Agent-based region growing for individual tree crown delineation from airborne laser scanning (ALS) data. *Int. J. Remote Sens.* **2015**, *36*, 1965–1993. [CrossRef]
24. Lahivaara, T.; Seppanen, A.; Kaipio, J.P.; Vauhkonen, J.; Korhonen, L.; Tokola, T.; Maltamo, M. Bayesian approach to tree detection based on airborne laser scanning data. *IEEE Trans. Geosci. Remote Sens.* **2014**, *52*, 2690–2699. [CrossRef]
25. Leckie, D.G.; Gougeon, F.A.; Tinis, S.; Nelson, T.; Burnett, C.N.; Paradine, D. Automated tree recognition in old growth conifer stands with high resolution digital imagery. *Remote Sens. Environ.* **2005**, *94*, 311–326. [CrossRef]
26. Chen, X.; Jiang, K.; Zhu, Y.; Wang, X.; Yun, T. Individual tree crown segmentation directly from UAV-Borne LiDAR data using the PointNet of deep learning. *Forests* **2021**, *12*, 131. [CrossRef]

27. Chen, Q.; Baldocchi, D.; Gong, P.; Kelly, M. Isolating individual trees in a savanna woodland using small footprint LiDAR data. *Photogramm. Eng. Remote Sens.* **2006**, *72*, 923–932. [CrossRef]
28. Wu, B.; Yu, B.; Wu, Q.; Huang, Y.; Chen, Z.; Wu, J. Individual tree crown delineation using localized contour tree method and airborne LiDAR data in coniferous forests. *Int. J. Appl. Earth Obs. Geoinf.* **2016**, *52*, 82–94. [CrossRef]
29. Hui, Z.; Li, N.; Cheng, P.; Li, Z.; Cai, Z. Single tree segmentation method for terrestrial LiDAR point cloud based on connectivity marker optimization. *Chin. J. Lasers* **2023**, *50*, 147–155. [CrossRef]
30. Wang, X.-H.; Zhang, Y.-Z.; Xu, M.-M. A multi-threshold segmentation for tree-level parameter extraction in a deciduous forest using small-footprint airborne LiDAR data. *Remote Sens.* **2019**, *11*, 2109. [CrossRef]
31. Wang, X.; Huang, Y.; Xing, Y.; Li, D.; Zhao, X. The single tree segmentation of UAV high-density LiDAR point cloud data based on coniferous plantations. *J. Cent. South Univ. For. Technol.* **2022**, *42*, 66–77. [CrossRef]
32. Ma, K.; Xiong, Y.; Jiang, F.; Chen, S.; Sun, H. A novel vegetation point cloud density tree-segmentation model for overlapping crowns using UAV LiDAR. *Remote Sens.* **2021**, *13*, 1442. [CrossRef]
33. Li, W.; Guo, Q.; Jakubowski, M.K.; Kelly, M. A new method for segmenting individual trees from the LiDAR point cloud. *Photogramm. Eng. Remote Sens.* **2012**, *78*, 75–84. [CrossRef]
34. Morsdorf, F.; Meier, E.; Allgwer, B.; Uesch, D. Clustering in airborne laser scanning raw data for segmentation of single trees. *Int. Arch. Photogramm. Remote Sens. Spat. Inf. Sci.* **2003**, *34*, W13.
35. Polewski, P.; Yao, W.; Heurich, M.; Krzystek, P.; Stilla, U. Detection of fallen trees in ALS point clouds using a normalized cut approach trained by simulation. *ISPRS J. Photogramm. Remote Sens.* **2015**, *105*, 252–271. [CrossRef]
36. Wu, J.; Cawse Nicholson, K.; Aardt, J.V. 3D tree reconstruction from simulated small footprint waveform LiDAR. *Photogramm. Eng. Remote Sens.* **2013**, *79*, 1147–1157. [CrossRef]
37. Yan, W.; Guan, H.; Cao, L.; Yu, Y.; Li, C.; Lu, J. A self-adaptive mean shift tree-segmentation method using UAV LiDAR data. *Remote Sens.* **2020**, *12*, 515. [CrossRef]
38. Liu, H.; Fan, W.; Xu, Y.; Lin, W. Research on single tree segmentation based on UAV LiDAR point cloud data. *J. Cent. South Univ. For. Technol.* **2022**, *42*, 45–53.
39. Paris, C.; Valduga, D.; Bruzzone, L. A hierarchical approach to three-dimensional segmentation of LiDAR data at single-tree level in a multilayered forest. *IEEE Trans. Geosci. Remote Sens.* **2016**, *54*, 4190–4203. [CrossRef]
40. Yang, J.; Kang, Z.; Cheng, S.; Yang, Z.; Akwensi, P.H. An individual tree segmentation method based on watershed algorithm and three-dimensional spatial distribution analysis from airborne LiDAR point clouds. *IEEE J. Sel. Top. Appl. Earth Observ. Remote Sens.* **2020**, *13*, 1055–1067. [CrossRef]
41. Ma, Z.; Pang, Y.; Wang, D.; Liang, X.; Lu, H. Individual tree crown segmentation of a larch plantation using airborne laser scanning data based on region growing and canopy morphology features. *Remote Sens.* **2020**, *12*, 1078. [CrossRef]
42. Nie, S.; Wang, C.; Xi, X.; Luo, S.; Zhu, X.; Li, G.; Liu, H.; Tian, J.; Zhang, S. Assessing the Impacts of Various Factors on Treetop Detection Using LiDAR-Derived Canopy Height Models. *IEEE Trans. Geosci. Remote Sens.* **2019**, *57*, 10099–10115. [CrossRef]
43. Khosravipour, A.; Skidmore, A.K.; Wang, T.; Isenburg, M.; Khoshelham, K. Effect of slope on treetop detection using a LiDAR Canopy Height Model. *ISPRS J. Photogramm. Remote Sens.* **2015**, *104*, 44–52. [CrossRef]
44. Stroner, M.; Urban, R.; Kremen, T.; Braun, J. UAV DTM acquisition in a forested area—Comparison of low-cost photogrammetry (DJI Zenmuse P1) and LiDAR solutions (DJI Zenmuse L1). *Eur. J. Remote Sens.* **2023**, *56*, 2179942. [CrossRef]
45. Zhao, X.; Guo, Q.; Su, Y.; Xue, B. Improved progressive TIN densification filtering algorithm for airborne LiDAR data in forested areas. *ISPRS J. Photogramm. Remote Sens.* **2016**, *117*, 79–91. [CrossRef]
46. Zhao, F.; Li, Z.; Wang, Y.; Pang, Y. The application of LiDAR data in forest. *Remote Sens. Inf.* **2008**, *18*, 106–108.
47. Popescu, S.C.; Wynne, R.H.; Nelson, R.F. Measuring individual tree crown diameter with LiDAR and assessing its influence on estimating forest volume and biomass. *Can. J. Remote Sens.* **2003**, *29*, 564–577. [CrossRef]
48. Jing, L.; Hu, B.; Noland, T.; Li, J. An individual tree crown delineation method based on multi-scale segmentation of imagery. *ISPRS J. Photogramm. Remote Sens.* **2012**, *70*, 88–98. [CrossRef]
49. Xu, W.; Yang, H.; Li, Z.; Cheng, J.; Lin, H.; Yang, G. Single tree segmentation in close-planting orchard using UAV digital image. *Geomat. Inf. Sci. Wuhan Univ.* **2022**, *47*, 1906–1916.